

SpectralNET: Exploring Spatial-Spectral WaveletCNN for Hyperspectral Image Classification

Tanmay Chakraborty and Utkarsh Trehan
MALIS - Machine Learning and Intelligent Systems
Lecturer: Dr. Maria A. Zuluaga

Department of Data Science and Engineering, EURECOM, Biot, France.
Emails: tanmay.chakraborty@eurecom.fr, utkarsh.trehan@eurecom.fr

Abstract—Hyperspectral Image (HSI) classification using Convolutional Neural Networks (CNN) is widely found in the current literature. Approaches vary from using SVMs to 2D CNNs, 3D CNNs, 3D-2D CNNs. Besides 3D-2D CNNs and FuSENet, the other approaches do not consider both the spectral and spatial features together for HSI classification task, thereby resulting in poor performances. 3D CNNs are computationally heavy and are not widely used, while 2D CNNs do not consider multi-resolution processing of images, and only limits itself to the spatial features. Even though 3D-2D CNNs try to model the spectral and spatial features their performance seems limited when applied over multiple dataset. In this article, we propose SpectralNET, a wavelet CNN, which is a variation of 2D CNN for multi-resolution HSI classification. A wavelet CNN uses layers of wavelet transform to bring out spectral features. Computing a wavelet transform is lighter than computing 3D CNN. The spectral features extracted are then connected to the 2D CNN which bring out the spatial features, thereby creating a spatial-spectral feature vector for classification. Overall a better model is achieved that can classify multi-resolution HSI data with high accuracy. Experiments performed with SpectralNET on benchmark dataset, i.e. Indian Pines, University of Pavia, and Salinas Scenes confirm the superiority of proposed SpectralNET with respect to the state-of-the-art methods. The code is publicly available in <https://github.com/tanmay-ty/SpectralNET>.

Keywords—Wavelet CNN; 2-D Convolutional Neural Net (CNN); 3-D Convolutional Neural Net; SpectralNET; hyperspectral image (HSI); spectral-spatial features; HSI classification.

I. INTRODUCTION

A Hyperspectral Image (HSI) is a high dimension image cube, where each band stores the intensity values of the pixels in a particular spectrum [1]. HSI classification is the task of correctly predicting the different pixel values associated with the different classes present in a remotely sensed HSI. Applications include urban development, detection of land changes, military applications, land cover analysis, crop detection etc. A key feature of HSI is they contain both spectral and spatial information.

Deep-learning based methods specially CNNs perform extremely well on image data. In recent works, HSI classification using different CNN models is also seen besides traditional hand-extracted feature based models [2]. Most models are based on 2D CNN, and 3D CNN [3]. Due to satisfactory performances of the two independent models [4], hybrid 3D-2D CNNs have also been proposed in the literature [5].

FuSENet is another model proposed in literature for HSI classification [6].

In [7], a band weighing strategy has been proposed that utilizes multiple binary support vector machines (SVM) in order to maximize the spectral distances between each class of a remotely sensed HSI. Their method was able to weight the spectral bands and improve classification results. A similar approach using SVMs has been proposed in [8], where the authors explored discrete space model (DSM) to transform continuous spectral features into discrete feature space, they utilized a composite kernel to take into account the spectral and spatial features. This pre-processing step improved the performance of SVMs for HSI classification. Kernel based approaches has also been found in the literature. In [9], spectral similarity based kernels has been developed and utilized along with the RBF kernel in a SVM. For the problem in hand they concluded spectral similarity based kernels outperform traditional SVM kernels.

The work in [10], adapts and improves the traditional low-rank representation (LRR) to the HSI classification problem. Locality-and structure-regularized LRR combines both the spectral and spatial features to explore the local similarity of pixels. The authors of [11], applied the concept of spectral gradient for HSI classification. They extracted the spatial features through a random forest algorithm and spectral features through spectral gradients. Then they perform a multi-scale fusion to integrate spatial-spectral features for the SVM to perform classification. The work in [12], introduced deep support vector machines (DSVM) for HSI classification. The model was able to outperform most of the state-of-the-art algorithms including all the variants of traditional SVMs.

In [13], a 3D octave CNN has been proposed which factorizes the mixed frequency feature map to reduce the spatial redundancy obtained when using a traditional 3D CNN with HSI. The authors of [14], utilized pseudo 3D blocks with a densely connected network. Their pseudo 3D blocks can capture both spectral and spatial features simultaneously compared to a traditional 3D CNN. The article [15], utilized small 3D patches extracted from the original HSI cube to train a 3D CNN with 3D kernel. In the following works [16], residual connections were added to a 3D CNN in order to assimilate both high and low level features present in a HSI and improve classification results. The work of [17], studied the effect of dimensionality reduction of HSI on 3D CNNs.

They concluded reducing the dimension of the training image reduced training time by 60%.

In [18], a 3D-2D CNN has been proposed for HSI classification. As a pre-processing the authors utilized channel wise shift and channel wise weighting to highlight the different spectral bands. In [4], 2D-3D CNN has been utilized with multi band feature fusion mechanism. This mechanism allows them to fuse both shallow and deep features in spectral band, which improves the feature vector sent into the dense layer. The work proposed in [19], introduces adaptive spectral unmixing into a 3D-2D CNN along with a early exit strategy. The early exit strategy reduces computational cost for easy samples. In [20], a residual hybrid 3D-2D CNN has been proposed, which has further been improved in [21] and is currently the state-of-the-art.

Efforts have also been made with Recurrent Neural Networks (RNN), Generative Adversarial Networks (GAN), Graph CNNs [22], and Squeeze and Excitation Residual Network [23]. RNNs consider the spectral signature of the HSI as a sequence in order to learn discriminative features [24].

Even though the 3D-2D CNNs model both the spatial and spectral features from a HSI cube, their model performance when applied over multiple dataset seems limited. 3D CNNs are also computationally expensive over 2D CNNs. So a method involving only 2D CNN as well as the power of extracting both spatial and spectral features is desirable.

In this article, a 2D wavelet CNN has been proposed for HSI classification. The work in [25], established wavelet transform as a good feature extractor for HSI classification task. Thus fusing the wavelet transform into a 2D CNN model brings out both the spectral and spatial features from a HSI. These features are then concatenated channel wise and sent as an input to the dense classification layers of the 2D CNN. The developed model uses Factor Analysis (FA) as a pre-processing step to reduce the huge dimensionality of HSI. Then patches are extracted and sent into the CNN. This reduces the training time as well. The spectral features coming from wavelet transform are computationally lighter as well compared to a 3D CNN. The model outperforms all previous models and paves the way for wavelet CNN in multi-resolution image classification. This model has been named *SpectralNET* in this paper.

The rest of the paper is arranged in the following way Section II, describes the *SpectralNET* model in details, Section III contains our experiments and discussions, and the paper is concluded in Section IV.

II. SPECTRALNET

The conventional 2D CNN can be considered a limited version of a multi-resolution CNN that can consider both spectral and spatial information [26]. Previous works have been successful in establishing the convolution and pooling function in a 2D CNN as filtering and downsampling [27]. A basic CNN can be mathematically represented as the weighed sum of nearest neighbours with an added constant bias.

A. Background for SpectralNET

Given an input vector X_n with corresponding labels Y_n from the \mathbb{R}^n space. In equation 1, Y_i is a label from Y_n labels and X_i is the corresponding sample from X_n . W_j is the weight defined by a filtering kernel. N_i are neighbouring i data.

$$y_i = \sum_{j \in N_i} W_j X_j \quad (1)$$

The equation 1 can be simply considered as the convolution of X_i and kernel W_j and can be rewritten as $\mathbf{Y} = \mathbf{X} * \mathbf{W}$. This is called the convolution layer of a CNN, where \mathbf{W} is in \mathbb{R}^o . The output of the convolution layers are typically big and needs to be pooled down before feeding it to the next layer. The pooling layers are placed in between convolution layers to perform a filtering operation and reducing the number of outputs.

This paves the way towards the multi-resolution CNN where the convolution is performed by a pair of kernels \mathbf{k}_{low} and \mathbf{k}_{high} which generate \mathbf{X}_{low} and \mathbf{X}_{high} . The multi-resolution CNN performs the hierarchical decomposition of the $\mathbf{X}_{\text{low},t}$ into $\mathbf{X}_{\text{low},t+1}$ and $\mathbf{X}_{\text{high},t+1}$ with different kernels at each step t .

For *SpectralNET*, the wavelet kernel $\mathbf{K}_{\text{high},t}$ is Haar wavelets and $\mathbf{K}_{\text{low},t}$ is a scaling function [28]. The 2D haar wavelets utilize the following four kernels ($f_{L,L}, f_{L,H}, f_{H,L}, f_{H,H}$) for wavelet transform [29].

$$\begin{aligned} f_{L,L} &= \begin{bmatrix} 1 & 1 \\ 1 & 1 \end{bmatrix} f_{L,H} = \begin{bmatrix} -1 & -1 \\ 1 & 1 \end{bmatrix} \\ f_{H,L} &= \begin{bmatrix} -1 & 1 \\ -1 & 1 \end{bmatrix} f_{H,H} = \begin{bmatrix} 1 & -1 \\ -1 & 1 \end{bmatrix} \end{aligned} \quad (2)$$

A HSI patch \mathbf{x} with $S \times S$ dimensions when passed through a Haar transform the (i,j) -th spectrum position value can be written as $\text{Haar}(i,j) = x(2i-1, 2j-1) + x(2i-1, 2j) + x(2i, 2j-1) + x(2i, 2j)$.

The HSI patch taken as an input is decomposed by the wavelet transform into sub-bands, these sub-bands are then sent through a convolution layer to learn the spectral and location features. Note that the sub-bands indicated as high and low pass filters do not necessarily filter the spectral band in with high pass and low pass filter. The part of the sub-band is again decomposed in the next layer by the wavelet transform and sent into the convolution layer. This process is continued in each layer and the CNN continues to learn the spectral and spatial features from the HSI patch.

B. SpectralNET Model Description

The input HSI cube having dimension $\mathbf{M} \times \mathbf{N} \times \mathbf{R}$ is first sent into a layer of Factor Analysis (FA) to reduce the dimension into $\mathbf{M} \times \mathbf{N} \times \mathbf{B}$. Reducing the dimension reduces training time by 60% [17]. The output vector \mathbf{Y} having a dimension $\mathbf{1} \times \mathbf{M} \times \mathbf{N}$ take up a class from the available land cover categories denoted by \mathbf{C} . The spectral dimensions are preserved in FA, i.e. $\mathbf{M} \times \mathbf{N}$, just the bands are reduced from \mathbf{R} to \mathbf{B} . Using FA in HSI as a pre-processing step is extremely beneficial, as FA is able to describe the variability among the different correlated and

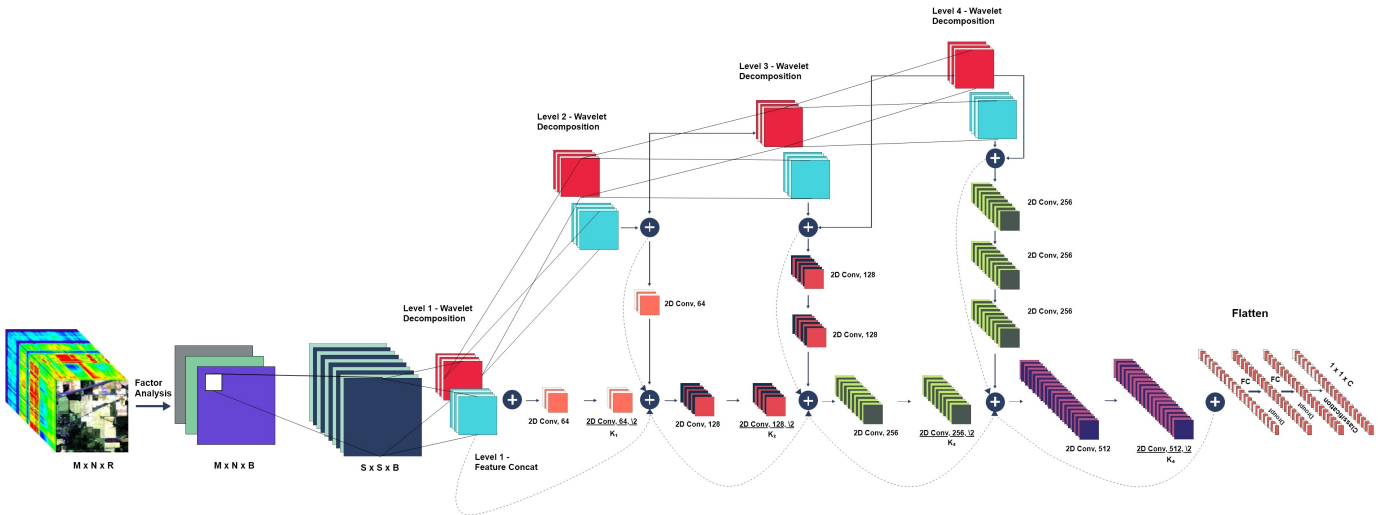


Fig. 1. Input HSI cube is pre-processed using Factor Analysis (FA) to reduce the dimension to 3. Patches are extracted from the pre-processed image and sent as an input to the SpectralNET model. SpectralNET model architecture with 4-level wavelet decomposition of the input HSI patch. The input kernel size is 3×3 with 1×1 padding. The output batch channel size is denoted by the numbers written after *conv*. To reduce feature map 3×3 kernels with stride 2 and 1×1 padding are used. The wavelet transformed features are added channelwise. To prevent the gradient from vanishing projection shortcuts are utilized with 1×1 convolutions. An average pooling layer is used globally after which the output is sent to the fully connected layers with dropout neurons.

overlapping spectrum bands, which helps making the model classify similar examples better. On the other hand, commonly used Principal Component Analysis (PCA) based reduction does not directly address this objective in HSI. PCA provides an approximation to the required factors which do not help to differentiate similar examples that well. After the FA step is complete, overlapping 3D patches of size $S \times S \times B$ are extracted from the pre-processed HSI and sent into the SpectralNET. $S \times S$ is the window size for patch extraction, for the Indian Pines dataset the patch size has been set at 64×64 and for the University of Pavia and Salinas Scene dataset the window size has been set at 24×24 . The truth values for these patches are determined by the center pixel's class category. The values were chosen based on experimentation to maximize the overall accuracy.

C. Implementation

The proposed *SpectralNET* model architecture is given in figure 1. The model is initialized with 3×3 convolution kernels and 1×1 padding. To replace pooling layers in between convolution a stride of 2 has been utilized. A global mean pooling has been employed at the end of all the convolution layers before sending into the dense layer, this prevents overfitting in the model. Dense connections has been utilized along with projection shortcuts for utilizing the wavelet transformed data more efficiently [30] [31]. Dense connections with channel wise concatenation of the decomposed data makes sure that all the features flow till the end of the model. The model explored two dropout layers as well along with batch normalization to prevent overfitting. Since the number of samples are very less in HSI the chances of overfitting are high. All steps to prevent the model from overfitting needs to be taken. Rectified Linear Unit (ReLU) has been utilized as the activation function.

TABLE I. DETAILED DESCRIPTION OF EACH DATASET USED DURING EXPERIMENT.

Name	Spatial Dimension	Spectral Bands	Wavelength Range	Classes
IP	145x145	224	400nm - 2500nm	16
UP	610x340	103	430nm - 860nm	9
SA	512x217	224	360nm - 2500nm	16

We explored the Stochastic gradient descent (SGD) over 150 epochs with a learning rate of 0.01 and momentum of 0.9 to optimize the objective function.

III. EXPERIMENTS, RESULTS, AND DISCUSSION

A. Dataset and Training

The experiments were conducted on multiple publicly available benchmark datasets, Indian Pines (IP), University of Pavia (UP), and Salinas Scene (SA)¹. The detailed descriptions of the three datasets are given in table I. The classification spectral layout for IP dataset is given in figure 2.

To perform the experiments, Google colab cloud platform with GPU has been utilized². Based on our experimental analysis an optimum learning rate of 0.01 with a momentum of 0.9 was chosen for the SGD optimizer. For preserving the validity of the results for all datasets, the bands of the extracted patches have all been set to 3. So, the patch dimension for IP dataset is $64 \times 64 \times 3$ and for UP and SA it is $24 \times 24 \times 3$ respectively. The model has been trained for 150 epochs and convergence was achieved at around 60 epochs.

B. Classification Results

The classification results are given in table II. Three benchmark metrics are utilized to judge the performance of the

¹<http://lesun.weebly.com/hyperspectral-data-set.html>

²<https://colab.research.google.com/>

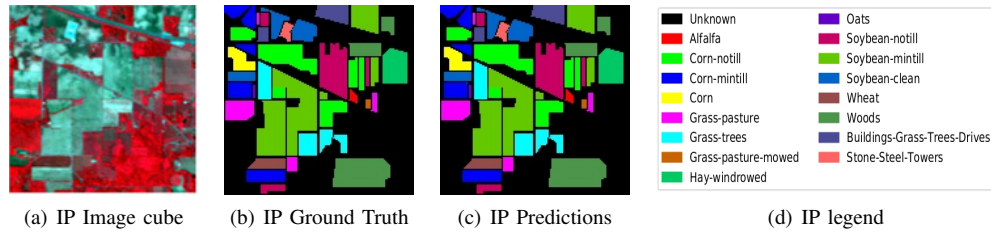


Fig. 2. Image cube, spectral ground truth, and spectral prediction for Indian Pines Dataset along with legend.

proposed model. Overall Accuracy (OA) gives the total number of correctly classified labels out of the total number of labels. Average Accuracy (AA) gives the mean of class wise classification accuracies, and Kappa Accuracy is a measure that correlates the ground truth and classified values. The results are compared with the state-of-the-art methods like HybridSN [21] and FuSENET [6], besides SVM, 2D CNN, 3D CNN, M3D CNN [32]³. The results are compared for two sets 10% - 90% random train test split and 30% - 70% random train test split respectively.

It can be observed from the results that the proposed model outperforms all state-of-the-art models in both the sets. Even though in the 10% train set the HybridSN model appears to perform better in SA dataset, that might be because of the fact it takes a lot more spectral bands as input compared to the proposed model. It can also be seen from the results that 2D CNN standalone performs better than 3D CNN in SA dataset. It might be due to the increased spectral redundancy in the SA dataset compared to the rest. The performance of FuSENET, HybridSN and *SpectralNET* is consistently high throughout the three dataset over M3D CNN. *SpectralNET* is able to outperform all even with a lot less spectral bands, i.e. 3, utilized than the state-of-the-art models which utilize 15, 30 bands. This highlights the merit of using wavelets based spectral features with a CNN. The time for training the *SpectralNET* is around 30 minutes which is also comparable to the currently established models.

For more detailed class wise classification results are in the appendix. From the results it can be established that the performance of *SpectralNET* is superior to all the methods currently available for HSI classification.

IV. CONCLUSION

In a nutshell, a wavelet CNN has been proposed in this work for HSI classification task. The developed *SpectralNET* takes into consideration both spectral and spatial features present in a high dimensional HSI cube using layers of wavelet decomposition of the input and adding that to the CNN. Experiments conducted with the three benchmark datasets IP, UP and SA along with a comparison with the state-of-the-art methods establish the superiority of the proposed model.

This work has been done in the context of the Machine Learning and Intelligent System (MALIS) course and it represents the final project report.

³<https://github.com/eeecn/Hyperspectral-Classification>

REFERENCES

- [1] J. M. Amigo, "Chapter 1.1 - hyperspectral and multispectral imaging: setting the scene," in *Hyperspectral Imaging* (J. M. Amigo, ed.), vol. 32 of *Data Handling in Science and Technology*, pp. 3 – 16, Elsevier, 2020.
- [2] S. Li, W. Song, L. Fang, Y. Chen, P. Ghamisi, and J. A. Benediktsson, "Deep learning for hyperspectral image classification: An overview," *IEEE Transactions on Geoscience and Remote Sensing*, vol. 57, no. 9, pp. 6690–6709, 2019.
- [3] X. Yang, Y. Ye, X. Li, R. Y. K. Lau, X. Zhang, and X. Huang, "Hyperspectral image classification with deep learning models," *IEEE Transactions on Geoscience and Remote Sensing*, vol. 56, no. 9, pp. 5408–5423, 2018.
- [4] Z. Ge, G. Cao, X. Li, and P. Fu, "Hyperspectral image classification method based on 2d–3d cnn and multi-branch feature fusion," *IEEE Journal of Selected Topics in Applied Earth Observations and Remote Sensing*, vol. 13, pp. 5776–5788, 2020.
- [5] M. Han, R. Cong, X. Li, H. Fu, and J. Lei, "Joint spatial-spectral hyperspectral image classification based on convolutional neural network," *Pattern Recognition Letters*, vol. 130, pp. 38 – 45, 2020. Image/Video Understanding and Analysis (IUVA).
- [6] S. K. Roy, "Fusenet: fused squeeze-and-excitation network for spectral-spatial hyperspectral image classification," *IET Image Processing*, vol. 14, pp. 1653–1661(8), June 2020.
- [7] C. Yan, X. Bai, P. Ren, L. Bai, W. Tang, and J. Zhou, "Band weighting via maximizing interclass distance for hyperspectral image classification," *IEEE Geoscience and Remote Sensing Letters*, vol. 13, no. 7, pp. 922–925, 2016.
- [8] L. Xie, G. Li, M. Xiao, L. Peng, and Q. Chen, "Hyperspectral image classification using discrete space model and support vector machines," *IEEE Geoscience and Remote Sensing Letters*, vol. 14, no. 3, pp. 374–378, 2017.
- [9] K. Wang, L. Cheng, and B. Yong, "Spectral-similarity-based kernel of svm for hyperspectral image classification," *Remote Sensing*, vol. 12, no. 13, p. 2154, 2020.
- [10] Q. Wang, X. He, and X. Li, "Locality and structure regularized low rank representation for hyperspectral image classification," *IEEE Transactions on Geoscience and Remote Sensing*, vol. 57, no. 2, pp. 911–923, 2019.
- [11] Z. Chunhui, G. Bing, Z. Lejun, and W. Xiaoqing, "Clas-

TABLE II. CLASSIFICATION ACCURACIES (%) OF PROPOSED SPECTRALNET IN TERMS OF OA, KAPPA, AND AA WITH VARYING TRAINING DATA 10% AND 30%, RESPECTIVELY

Training Samples	Methods	IP dataset			UP dataset			SA dataset		
		OA	Kappa	AA	OA	Kappa	AA	OA	Kappa	AA
10%	SVM	81.67±0.65	78.76±0.77	79.84±3.37	90.58±0.47	87.21±0.70	92.99±0.36	94.46±0.12	93.13±0.34	93.01±0.60
	2D-CNN	80.27±1.2	78.26±2.1	68.32±4.1	96.63±0.2	95.53±0.2	94.84±1.4	96.34±0.3	95.93±0.9	94.36±0.5
	3D-CNN	82.62±0.1	79.25±0.3	76.51±0.1	96.34±0.2	94.90±1.2	97.03±0.6	85.00±0.1	83.20±0.7	89.63±0.2
	M3D-CNN	81.39±2.6	81.20±2.0	75.22±0.7	95.95±0.6	93.40±0.4	97.52±1.0	94.20±0.8	93.61±0.3	96.66±0.5
	FuSENet	97.11±0.2	97.25±0.2	97.32±0.2	97.65±0.3	97.69±0.3	97.68±0.4	99.23±0.1	99.97±0.2	99.16±0.1
	HybridSN	98.39±0.1	98.16±0.1	98.01±0.2	99.72±0.1	99.64±0.1	99.20±0.1	99.98±0.2	99.98±0.2	99.98±0.1
	SpectralNET	98.76±0.2	98.59±0.1	98.61±0.1	99.71±0.1	99.62±0.1	99.43±0.2	99.96±0.2	99.96±0.1	99.97±0.1
30%	SVM	87.24±0.38	85.27±0.45	85.15±1.10	95.65±0.13	94.63±0.17	94.60±0.14	94.95±0.10	94.48±0.11	97.93±0.11
	2D-CNN	88.90±1.3	87.01±1.6	85.70±1.0	96.50±0.4	96.55±0.3	96.00±0.1	96.75±0.6	96.71±0.7	98.57±0.2
	3D-CNN	90.23±0.2	89.70±0.3	89.87±0.1	97.90±0.3	97.22±0.1	97.30±0.1	95.54±0.5	94.81±0.3	97.09±0.6
	M3D-CNN	95.67±0.1	94.70±0.3	94.60±0.6	97.60±0.2	96.50±0.6	98.00±0.1	94.99±0.3	95.40±0.1	96.28±0.2
	FuSENet	99.01±0.2	98.60±0.1	98.64±0.1	99.42±0.2	99.21±0.3	99.33±0.2	99.68±0.2	99.74±0.1	99.69±0.1
	HybridSN	99.75±0.1	99.71±0.1	99.63±0.2	99.98±0.1	99.98±0.2	99.97±0.2	100	100	100
	SpectralNET	99.86±0.2	99.84±0.2	99.98±0.1	99.99±0.1	99.98±0.1	99.98±0.1	100	100	100

sification of hyperspectral imagery based on spectral gradient, svm and spatial random forest,” *Infrared Physics and Technology*, vol. 95, pp. 61 – 69, 2018.

- [12] O. Okwuashi and C. E. Ndehedehe, “Deep support vector machine for hyperspectral image classification,” *Pattern Recognition*, vol. 103, p. 107298, 2020.
- [13] Q. Xu, Y. Xiao, D. Wang, and B. Luo, “Csa-mso3dcnn: Multiscale octave 3d cnn with channel and spatial attention for hyperspectral image classification,” *Remote Sensing*, vol. 12, no. 1, p. 188, 2020.
- [14] A. Li and Z. Shang, “A new spectral-spatial pseudo-3d dense network for hyperspectral image classification,” in *2019 International Joint Conference on Neural Networks (IJCNN)*, pp. 1–7, 2019.
- [15] M. Ahmad, “A fast 3d cnn for hyperspectral image classification,” 2020.
- [16] Z. Zhong, J. Li, Z. Luo, and M. Chapman, “Spectral-spatial residual network for hyperspectral image classification: A 3-d deep learning framework,” *IEEE Transactions on Geoscience and Remote Sensing*, vol. 56, no. 2, pp. 847–858, 2018.
- [17] N. Laban, B. Abdellatif, H. M. Ebeid, H. A. Shedeed, and M. F. Tolba, “Reduced 3-d deep learning framework for hyperspectral image classification,” in *The International Conference on Advanced Machine Learning Technologies and Applications (AMLTA2019)* (A. E. Hassanien, A. T. Azar, T. Gaber, R. Bhatnagar, and M. F. Tolba, eds.), (Cham), pp. 13–22, Springer International Publishing, 2020.
- [18] J. Zheng, Y. Feng, C. Bai, and J. Zhang, “Hyperspectral image classification using mixed convolutions and covariance pooling,” *IEEE Transactions on Geoscience and Remote Sensing*, pp. 1–13, 2020.
- [19] B. Fang, Y. Bai, and Y. Li, “Combining spectral unmixing and 3d/2d dense networks with early-exiting strategy for hyperspectral image classification,” *Remote Sensing*, vol. 12, no. 5, p. 779, 2020.
- [20] F. Feng, S. Wang, C. Wang, and J. Zhang, “Learning deep hierarchical spatial-spectral features for hyperspectral image classification based on residual 3d-2d cnn,” *Sensors*, vol. 19, no. 23, p. 5276, 2019.
- [21] S. K. Roy, G. Krishna, S. R. Dubey, and B. B. Chaudhuri, “Hybridsn: Exploring 3-d-2-d cnn feature hierarchy for hyperspectral image classification,” *IEEE Geoscience and Remote Sensing Letters*, vol. 17, no. 2, pp. 277–281, 2020.
- [22] L. Mou, X. Lu, X. Li, and X. X. Zhu, “Nonlocal graph convolutional networks for hyperspectral image classification,” *IEEE Transactions on Geoscience and Remote Sensing*, pp. 1–12, 2020.
- [23] L. Wang, J. Peng, and W. Sun, “Spatial-spectral squeeze-and-excitation residual network for hyperspectral image classification,” *Remote Sensing*, vol. 11, no. 7, p. 884, 2019.
- [24] R. Hang, Q. Liu, D. Hong, and P. Ghamisi, “Cascaded recurrent neural networks for hyperspectral image classification,” *IEEE Transactions on Geoscience and Remote Sensing*, vol. 57, no. 8, pp. 5384–5394, 2019.
- [25] T. N. Prabhakar and P. Geetha, “Two-dimensional empirical wavelet transform based supervised hyperspectral image classification,” *ISPRS Journal of Photogrammetry and Remote Sensing*, vol. 133, pp. 37 – 45, 2017.
- [26] S. Fujieda, K. Takayama, and T. Hachisuka, “Wavelet convolutional neural networks,” *arXiv preprint arXiv:1805.08620*, 2018.
- [27] S. Fujieda, K. Takayama, and T. Hachisuka, “Wavelet convolutional neural networks for texture classification,” *arXiv preprint arXiv:1707.07394*, 2017.
- [28] X. Wang, “Moving window-based double haar wavelet transform for image processing,” *IEEE Transactions on image processing*, vol. 15, no. 9, pp. 2771–2779, 2006.
- [29] P. Liu, H. Zhang, K. Zhang, L. Lin, and W. Zuo, “Multi-level wavelet-cnn for image restoration,” in *Proceedings of the IEEE conference on computer vision and pattern recognition workshops*, pp. 773–782, 2018.
- [30] K. He, X. Zhang, S. Ren, and J. Sun, “Deep residual learning for image recognition,” in *Proceedings of the IEEE conference on computer vision and pattern recognition*, pp. 770–778, 2016.
- [31] G. Huang, Z. Liu, L. Van Der Maaten, and K. Q. Weinberger, “Densely connected convolutional networks,” in *Proceedings of the IEEE conference on computer vision and pattern recognition*, pp. 4700–4708, 2017.
- [32] M. He, B. Li, and H. Chen, “Multi-scale 3d deep convolutional neural network for hyperspectral image classification,” in *2017 IEEE International Conference on Image Processing (ICIP)*, pp. 3904–3908, 2017.

APPENDIX CLASSWISE CLASSIFICATION RESULTS

Class wise classification results for IP, SA and UP datasets are summarised in table III, IV, and V respectively. Confusion matrix are available in figure 3.

TABLE III. DETAILED CLASSIFICATION RESULTS FOR INDIAN PINES DATASET IN TERMS OF PRECISION, RECALL, F1-SCORE, TEST LOSS, OVERALL ACCURACY, AVERAGE ACCURACY AND KAPPA ACCURACY.

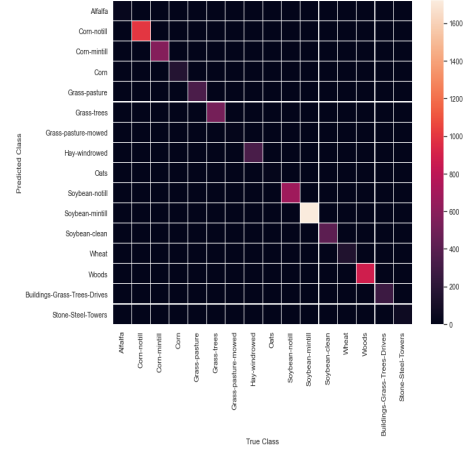
Class Labels	Precision	Recall	f1-score	Support
Alfalfa	1.00	1.00	1.00	32
Corn-notill	1.00	1.00	1.00	1000
Corn-mintill	1.00	0.99	1.00	581
Corn	1.00	1.00	1.00	166
Grass-pasture	0.99	1.00	1.00	338
Grass-trees	1.00	1.00	1.00	511
Grass-pasture-mowed	1.00	0.85	0.92	20
Hay-windrowed	1.00	1.00	1.00	335
Oats	0.78	1.00	0.88	14
Soybean-notill	1.00	1.00	1.00	680
Soybean-mintill	1.00	1.00	1.00	1719
Soybean-clean	1.00	1.00	1.00	415
Wheat	1.00	1.00	1.00	143
Woods	1.00	1.00	1.00	886
Buildings-Grass-Trees-Drives	1.00	1.00	1.00	270
Stone-Steel-Towers	0.98	1.00	0.99	65
accuracy			1.00	7175
macro avg	0.98	0.99	0.99	7175
weighted avg	1.00	1.00	1.00	7175
Test loss				0.7%
Average accuracy (%)				99.98%
Kappa accuracy (%)				99.84%
Overall accuracy (%)				99.86%

TABLE IV. DETAILED CLASSIFICATION RESULTS FOR SALINAS SCENE DATASET IN TERMS OF PRECISION, RECALL, F1-SCORE, TEST LOSS, OVERALL ACCURACY, AVERAGE ACCURACY AND KAPPA ACCURACY.

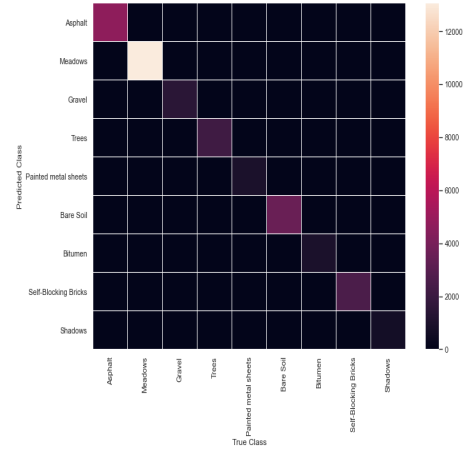
Class Labels	Precision	Recall	f1-score	Support
Brocoli-green-weeds-1	1.00	1.00	1.00	1406
Brocoli-green-weeds-2	1.00	1.00	1.00	2608
Fallow	1.00	1.00	1.00	1383
Fallow-rough-plow	1.00	1.00	1.00	976
Fallow-smooth	1.00	1.00	1.00	1875
Stubble	1.00	1.00	1.00	2771
Celery	1.00	1.00	1.00	2505
Grapes-untrained	1.00	1.00	1.00	7890
Soil-vinyard-develop	1.00	1.00	1.00	4342
Corn-senesced-green-weeds	1.00	1.00	1.00	2295
Lettuce-romaine-4wk	1.00	1.00	1.00	748
Lettuce-romaine-5wk	1.00	1.00	1.00	1349
Lettuce-romaine-6wk	1.00	1.00	1.00	641
Lettuce-romaine-7wk	1.00	1.00	1.00	749
Vinyard-untrained	1.00	1.00	1.00	5088
Vinyard-vertical-trellis	1.00	1.00	1.00	1265
accuracy	1.00	1.00	1.00	37891
macro avg	1.00	1.00	1.00	37891
weighted avg	1.00	1.00	1.00	37891
Test loss				0.001%
Average accuracy (%)				100%
Kappa accuracy (%)				100%
Overall accuracy (%)				100%

TABLE V. DETAILED CLASSIFICATION RESULTS FOR UNIVERSITY OF PAVIA DATASET IN TERMS OF PRECISION, RECALL, F1-SCORE, TEST LOSS, OVERALL ACCURACY, AVERAGE ACCURACY AND KAPPA ACCURACY.

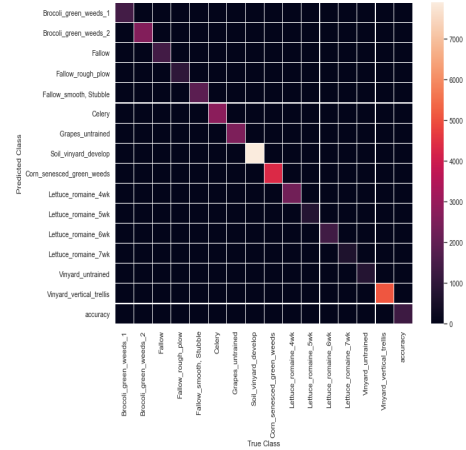
Class Labels	Precision	Recall	f1-score	Support
Asphalt	1.00	1.00	1.00	4642
Meadows	1.00	1.00	1.00	13055
Gravel	1.00	1.00	1.00	1496
Trees	1.00	1.00	1.00	2145
Painted metal sheet	1.00	1.00	1.00	942
Bare soil	1.00	1.00	1.00	3520
Bitumen	1.00	1.00	1.00	931
Self-Blocking Bricks	1.00	1.00	1.00	2577
Shadows	1.00	1.00	1.00	663
accuracy	1.00	1.00	1.00	29944
macro avg	1.00	1.00	1.00	29944
weighted avg	1.00	1.00	1.00	29944
Test loss				0.07%
Average accuracy (%)				99.98%
Kappa accuracy (%)				99.98%
Overall accuracy (%)				99.99%



(a) IP Confusion Matrix



(b) UP Confusion Matrix



(c) SA Confusion Matrix

Fig. 3. Confusion matrix for IP, UP, and SA using SpectralNET.